Chaos in Nonlinear Dynamical Systems

Interim Report on Vibration Mechanisms of the GKN EH101 Helicopter

James H. Taylor[1] and S. Salamat Sharif[2]
Department of Electrical and Computer Engineering
University of New Brunswick
Fredericton, N. B., CANADA, E3B 5A3
E-mail: 1) jtaylor@unb.ca, 2) salamat@ee.unb.ca

Prepared for:

GKN Westland Helicopters Ltd.

9 August 2001

Contents

Chaos in Nonlinear Dynamical Systems

James H. Taylor and S. Salamat Sharif

University of New Brunswick

9 August 2001

Abstract

The nonlinear dynamic behaviour of the GKN EH101 Helicopter is considered in this preliminary report. The main objective of this study is to characterize the helicopter vibration mechanism(s) and the appropriate way to control them. This report is based on analyses of GKN EH101 Helicopter flight data, specifically acceleration for two different airspeeds with a sampling rate of 1024 Hz.

This report deals with the possible presence of chaotic behaviour in the flight data. Some background in the theory of chaos in nonlinear dynamical systems is discussed, and approaches for the identification of chaos in flight data are presented. Several topics including delay-coordinate embedding theory, delay time and dimension calculation, and Lyapunov exponent computation for chaotic systems are described. In each section, the GKN flight data set is analyzed and examined. Finally, implications regarding the possibility of chaotic behaviour in the flight data are discussed, and the next steps in this study are presented.

1 Introduction

An understanding of the identification and control of chaotic systems has improved tremendously in the last decade [1]-[22]. Chaotic behaviour occurs in systems with nonlinear dynamics. The recognition of chaos in a complex dynamical system is very complicated. An important characteristic of a chaotic system is its sensitive dependence on initial conditions. The trajectories of such systems can be completely different even for very close initial conditions. This factor makes the predictability of these systems very difficult and even impossible in the long run. It also introduces new and challenging problems in the area of control.

In many cases, the chaotic behaviour of a system may be mistaken for randomness or noise effects. A system with nonlinearity and random inputs can certainly produce irregular trajectories. However, a random input is not the only possible source of irregular behaviour in a system; nonlinear chaotic systems can have very irregular output with purely deterministic dynamics and inputs. One important issue in such systems is the discrimination of chaos from randomness. This factor also has very important implications for controlling nonlinear systems. If a system shows some signs of chaotic behaviour, then it may be controlled with some of the methods which

are proposed in the literature [6, 8, 10, 13, 14, 15].

Chaos may exist in classical systems (represented by mathematical models) or real-life systems. Examples of classical systems include the logistic, tent and Hénon maps in the realm of discrete systems, and the Lorenz and Rössler differential equations for continuous-time dynamical systems [2]. Some real-life systems in which chaos has been identified are complex chemical reactions, pendula with periodic forcing functions [2], NMR laser data, human breath rate, vibrating spring data, foetal electrocardiogram signals [8], among others.

In most real-life systems, system behaviour is characterized by time series data available from measurement. For this reason, useful methods for analyzing these systems should be able to deal with time series data. These data can be measurements of only one variable, or measurements of several variables. The first step in the analysis of time series data was introduced in *Geometry from a time series* [16], in which state space reconstruction of time series data was proposed for the first time. The mathematical justification of this approach was presented in [22]. Based on a mathematical proof given in [22], the reconstructed state space is diffeomorphically (one-to-one and invertible) equivalent to the original state space of the real-life system.

In delay-coordinate reconstruction, the selection of time delay and dimension are the most important issues [5, 9, 11, 12, 20]. For the calculation of time lag, different approaches are proposed in the literature [5, 11]. Among them, the autocorrelation function and mutual information approach are the most common [15]. Among the different techniques of the calculation of embedding dimension, the "false nearest neighbours" method has attracted the most attention [9].

By appropriate selection of time delay and embedding dimension, the time series data can be reconstructed in the delay-coordinate state space. In this space, the chaotic behaviour of the nonlinear dynamical system can be studied. A common method for the identification of chaos in state space systems is to calculate the Lyapunov exponent [14]. The calculation of this exponent from time series data has been extensively considered in the literature [7, 17, 18].

The organization of this report is as follows. In Section 2, the delay-coordinate state space reconstruction of time series data is discussed. In Section 3, the calculation of the optimal time delay for delay-coordinate reconstruction is described and carried out. In Section 4, the dimension calculation of the reconstructed state space is addressed and also executed. In Section 5, the computation of Lyapunov exponent for time series data, and identification of chaos is considered and preliminary results presented. In Section 6, the concluding remarks about the GKN data and the possible presence of chaos are discussed.

2 Time Series and State Space Reconstruction via Delay-Coordinate Embedding

In most cases, observations of a system are in the form of time series data, not a state space representation. However, the more effective approaches for studying deterministic dynamical systems involve describing the system in an appropriate state space. For this reason, time series data should be converted into state space vectors. This procedure is known as *state space reconstruction*, which is based on a theorem attributed to Takens [22].

2.1 State Space Models

A state space is a finite-dimensional vector space, $\Re^m$. In this space, a state is shown by a vector $\mathbf{x} \in \Re^m$. In state space, the dynamics of the system can be presented by an m-dimensional *map*, $\mathbf{F}$, as:

$$\mathbf{x}_{n+1} = \mathbf{F}(\mathbf{x}_n, n), \tag{1}$$

where the index n denotes the discrete time instants; or by a *flow* (a system of m first-order ordinary differential equations) as:

$$\frac{d}{dt}\mathbf{x}(t) = \mathbf{f}(\mathbf{x}(t),\ t), \qquad t \in \Re. \tag{2}$$

If $\mathbf{F}$ does not depend on n, or $\mathbf{f}$ does not depend on t, then the map or flow is called *autonomous*; hereafter we will consider only that case. A sequence of points $\mathbf{x}_n$ solving Equation (1), or continuous solution $\mathbf{x}$(t) satisfying Equation (2), is called a *trajectory*, and $\mathbf{x}_0$ (or $\mathbf{x}(0)$) the *initial condition*. The orbit of $\mathbf{x}$ under $\mathbf{F}$ is the set of points $\{\mathbf{x},\ \mathbf{F}(\mathbf{x}),\ \mathbf{F}^2(\mathbf{x}),\ \cdots\}$, and the trajectory of $\mathbf{x}$(t) under $\mathbf{f}$ is the solution of the indicated ordinary differential equation, usually obtained by numerical integration.

Certain solutions or trajectories are particularly important in characterizing the behaviour of nonlinear dynamic systems; for non-chaotic systems these are *fixed points* and *closed trajectories* (period-K orbits or limit cycles). A fixed point $\mathbf{p}$ satisfies $\mathbf{F}(\mathbf{p}) = \mathbf{p}$ or $\mathbf{f}(\mathbf{p}) = 0$; in other words, if $\mathbf{x}_0 = \mathbf{p}$ in Equation (1), then $\mathbf{x}_n = \mathbf{p}$, $n = 1, 2, \ldots$, or, in Equation (2), $\mathbf{x}$(t) $\equiv \mathbf{p}$, $\forall t > 0$. Informally, a closed trajectory satisfies $\mathbf{x}_{n+K} = \mathbf{x}_n$ for some period-K or $\mathbf{x}(t) = \mathbf{x}(t + \tau)$ for some period τ. The period K is the minimum value for which $\mathbf{F}^K(\mathbf{x}) = \mathbf{x}$, and similarly τ is the smallest value for which $\mathbf{x}(t) = \mathbf{x}(t + \tau)$. A (non-chaotic) *attractor* of a system is a fixed point or closed trajectory such that for a set of near-by initial conditions the resulting solutions will be attracted to it after some transient time or, more commonly, as n or t approaches infinity. Non-chaotic attractors are stable fixed points and stable limit cycles. The set of initial conditions leading to the same attractor is called the attractor's *basin of attraction*. Note that the concept of attractor may also be extended

to systems with chaotic behaviour, but such a concept and definition is not required here.

For many physical systems, a state space flow model, Equation (2), is not available; rather, observations of the system variables are taken, including measurements of one or several quantities which depends on the current state of the system. Given a scalar signal, $s(t)$, regularly sampled at time interval τ_s starting at some time t_0, the nth sample can be represented as:

$$s_n = s(t_0 + (n-1)\tau_s) + \eta_n\,, \quad n = 1,\, 2,\, \ldots \tag{3}$$

where η_n is the measurement noise. A delay-coordinate reconstruction can be formed by plotting the time series versus a time-delayed version of it. For a 2-dimensional reconstruction, we plot the delay vector $\mathbf{y}(n) = (s_n, s_{n-V})$, where V is the *lag* or *sampling delay*, i.e., the difference between the adjacent components of the delay vector in number of samples. For a d-dimensional reconstruction, the delay vector, $\mathbf{y}(n)$ can be presented as:

$$\mathbf{y}(n) = [s_n, s_{n-V},\ \cdots,\ s_{n-(d-2)V},\ s_{n-(d-1)V}] \tag{4}$$

One of the major issues in the embedding approach is: Under what conditions is the trajectory of the reconstructed state space equivalent to the original trajectory $\mathbf{x}_n$? It was proved by Takens [22] that if the dimension of the delay-coordinate space, d, is sufficiently large, the attractor formed by the $\mathbf{y}(n)$ vector is equivalent to the attractor in the original space. Specifically, if the dimension of the reconstructed space, d, is larger than twice the *box counting dimension* m of the attractor (or the number of *active* degrees of freedom), the equivalence of the spaces is guaranteed. In some applications, a smaller value of d can also be sufficient [1]. Based on these results, if the dimension of the original attractor is not very high, the reconstruction is possible even if the dimension of the original system is very high. Systems with this characteristic include hydrodynamic flows and lasers [8].

The selection of d, the dimension of the state space reconstruction, and V, the sampling delay (or $T = V\tau_s$, the time lag), are of great importance, and needs detailed analysis. In many applications, the product $d \cdot V$ is the governing factor for the delay-coordinate reconstruction [10]. However, the separation of d and V makes their calculation easier.

The calculation of V and d are discussed in Sections 3 and 4, respectively. From a mathematical point of view, the selection of V has no effect on the embedding of a noise-free time series. However, in practical applications and for data contaminated with noise, a good choice of V has an important impact on the analysis [4]. If V is too small in comparison with the dynamic variation of the system, successive elements of the delay vectors are strongly correlated. If V is too large, successive elements are almost independent. Several approaches are proposed in the literature for the calculation of an optimal value of the sampling lag. Among these methods, the use

of the *autocorrelation function* and *mutual information* (see Section 3) are the most common. Optimal values of V can be verified through the visualization of the data in a two-dimensional embedding space.

2.2 GKN Time Series Data

The dynamical system which is considered in this report characterized by the flight data of the GKN helicopter EH101. Two set of data are examined, each comprised of acceleration signals (calibration withheld) for two different airspeeds (also withheld). The time series data are sampled at $f_s = 1024$ Hz in the nominal rotor speed of $f_n = 3.57$ Hz. The predominant frequency is the blade passing frequency of $5f_n$ at 17.85 Hz. The data are sampled when the active vibration control system is switched off.

In this report, the two sets of flight data are referred to as data-set one (GKN_1) and data-set two (GKN_2). The time evolution of the whole data sets and the first 1000 samples are shown in Figure 1 and 2, respectively.

As a preliminary investigation, the power spectrum of these data was also calculated; the results are presented in Figure 3. As shown in this figure, the highest amplitude pertains to the blade passing frequency of $5f_n = 17.85$ Hz; however, we observe that substantial power is also present over a broad range of frequencies. The general sources of broad band frequency content can be random noise or chaos; since the time series plots appear to be quite clean (Figure 2), the presence of chaos in the time series data may be suspected.

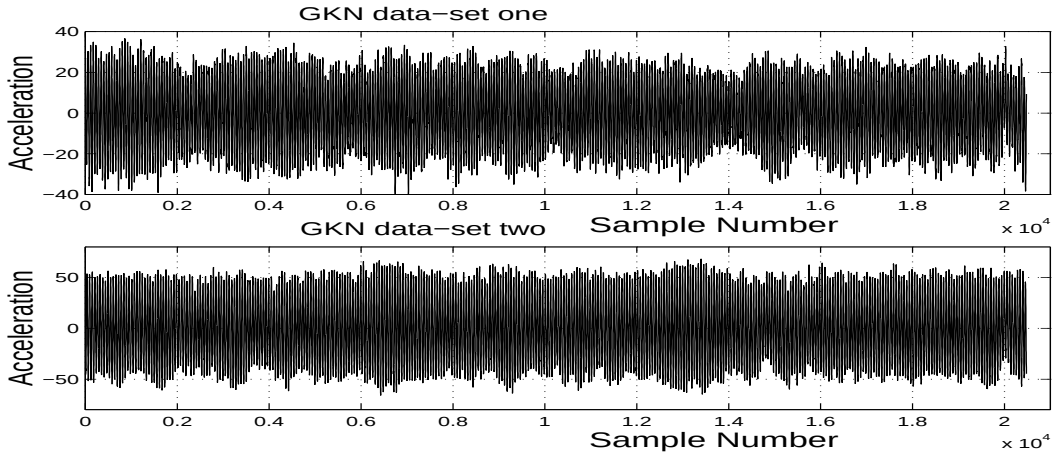

Figure 1: The time evolution of GKN data-set one and data-set two

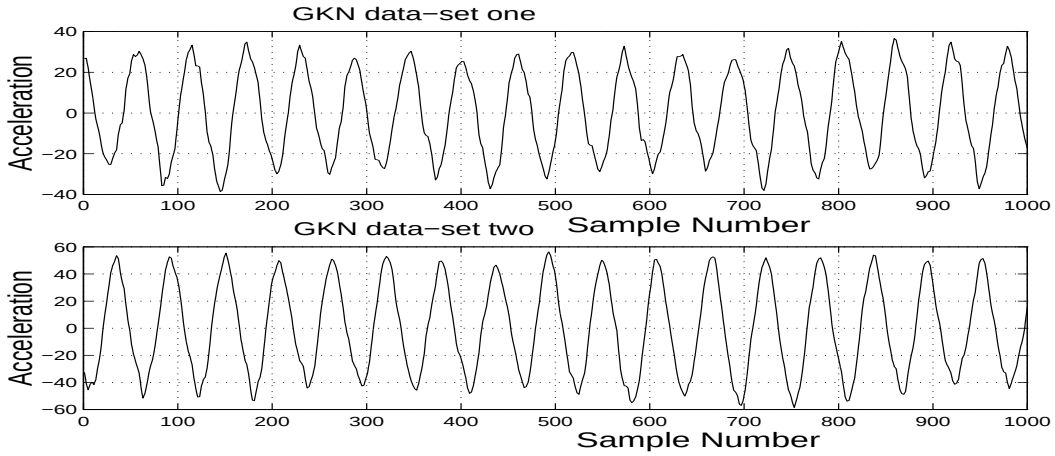

Figure 2: The time evolution of the first 1000 samples of GKN_1 and GKN_2

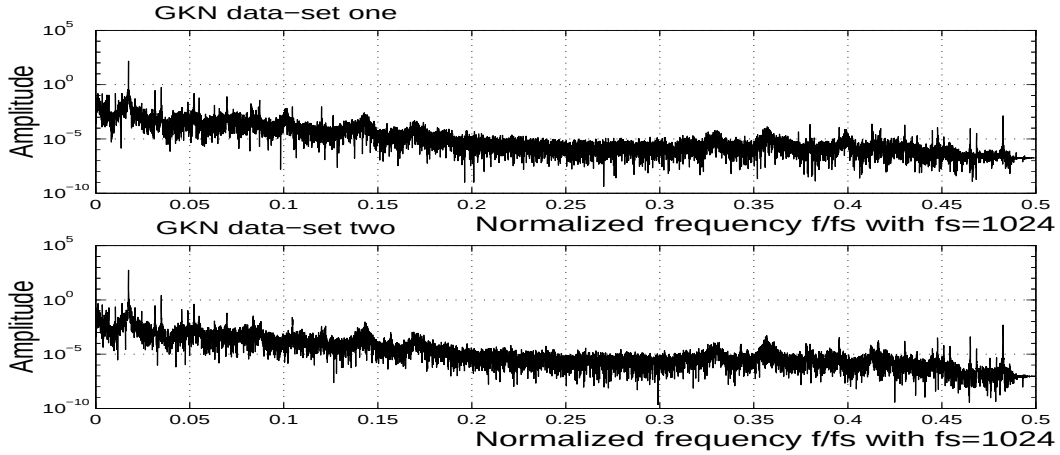

Figure 3: Power spectrum of GKN data-set one and data-set two

2.3 Hénon Map and Lorenz System

For the verification of the obtained results for the GKN flight data, two classical models are also addressed in this report. Hénon Map and Lorenz System, respectively as a discrete and continuous chaotic system are selected. The calculated values for these models are compared with the reported values in the literature, and very close conformation have been obtained. This conformation can give us some confidence about the accuracy of our analysis. The Hénon Map can be presented as:

$$\begin{cases} x_{n+1} = 1 - ax_n^2 + y_n \\ y_{n+1} = bx_n, \end{cases} \tag{5}$$

where a and b are equal to 1.4 and 0.3, respectively. The time evolution of Hénon Map in the 2-dimensional state space is illustrated in Figure 4. The Lorenz System

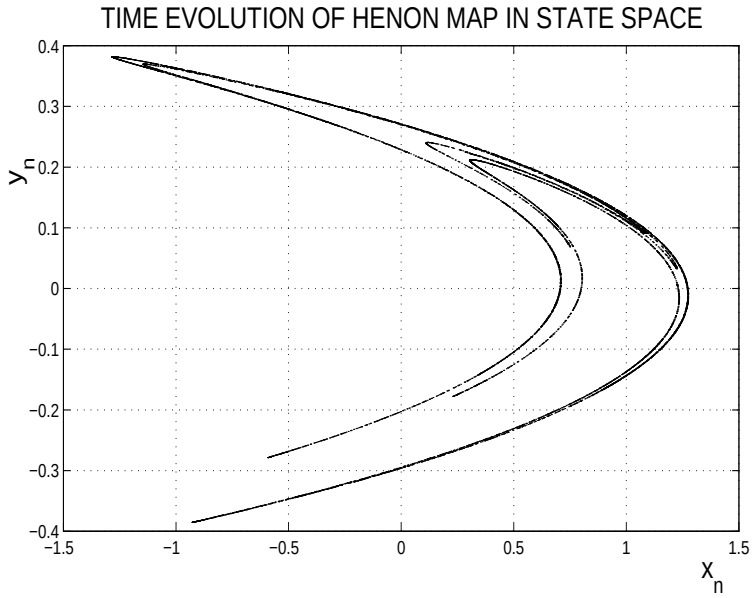

Figure 4: The time evolution of Hénon Map in the 2-dimensional state space

can be formulated as:

$$\begin{cases} \dot{x} = \sigma(y - x) \\ \dot{y} = x(R - z) - y \\ \dot{z} = xy - bz, \end{cases} \tag{6}$$

where $\sigma = 16.0$, $R = 45.92$, and $b = 4.0$. The three state variables of this system are two componenets of temperature and one component of velocity in the convection problem. For comparison of Lorenz System and the GKN time series data, the time evolution and power spectrum of the three states of this system are shown in Figure 5 and 6, respectively.

3 Calculation of Optimal Time Delay

From a mathematical point of view, if an infinite amount of infinitely accurate data is available, there is no limit on the choice of sampling delay, except certain multiples of the precise period of a periodic signal. These conditions cannot be met in real-life data, and an optimal choice of sampling delay plays an important role in the analysis of the reconstructed system. The selection of sampling delay, V, should primarily be based on the following considerations:

1. If the selected sampling delay is too short, the adjacent points (s_n and s_{n-V}) will not be sufficiently independent (will have almost the same information). This condition is also called redundancy [3]. In addition, if the data are noisy,

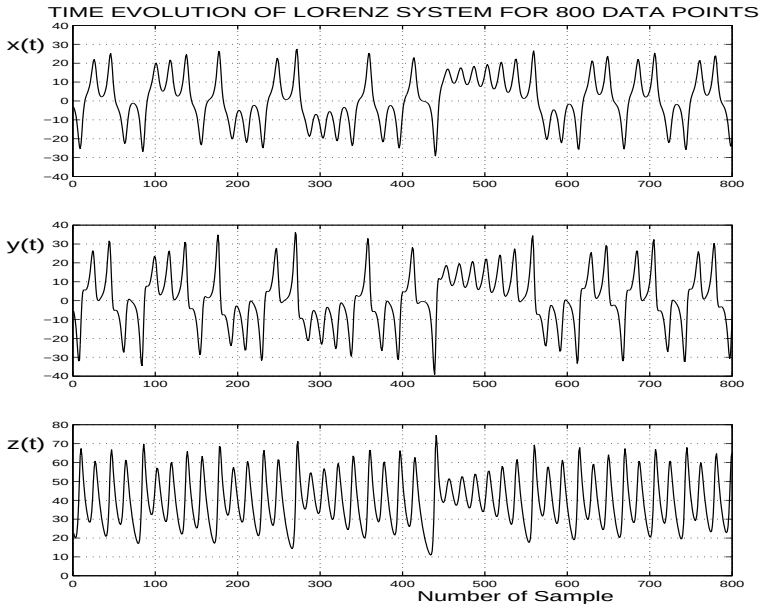

Figure 5: The time evolution of the three states of Lorenz System

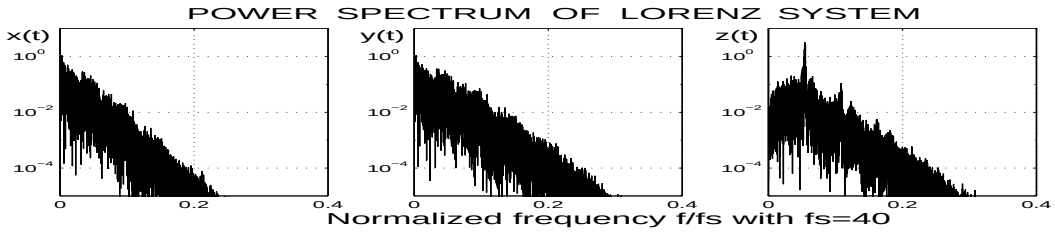

Figure 6: Power spectrum of the three states of Lorenz System

and the variation of the signal during the interval covered in vector $\mathbf{y}(n)$, $d \cdot V$, is less than the noise level, the vector will have no information.

2. If the sampling delay selected is too large, any relation between s_n and s_{n-V} can be regarded as randomness due to the sensitive nature of the chaos. This is the problem with chaotic systems, where the autocorrelation function decays very rapidly.

As a result, an optimal sampling delay should be large enough to give rather independent values for s_n and s_{n-V}, and not too large that it gives completely independent s_n and s_{n-V}. On the other hand, there is not an optimal value for the sampling delay from the mathematical point of view, as mentioned above. Techniques for the optimal selection of sampling delay have been discussed in the literature extensively. Many of these methods are appropriate only for a specified application. Here, two methods which give satisfactory results in most applications are discussed. These methods deal with the statistical behaviour of the signal, as explained below.

3.1 Time Delay Calculation: Autocorrelation Method

In this approach, the autocorrelation function of the signal is used to identify the optimal value of sampling delay. The autocorrelation function for each sampling delay V can be defined as follows:

$$C_T \;=\; \frac{\langle (s_n - \langle s \rangle)(s_{n-V} - \langle s \rangle) \rangle}{\sigma^2}, \tag{7}$$

where $\langle \cdot \rangle$ denotes ensemble average and $\langle s \rangle$ is the estimated mean of the signal; for a time series with N points this is equal to:

$$\langle s \rangle = \frac{\sum_{n=1}^{N} s_n}{N}, \tag{8}$$

and σ^2 is the variance of the time series, and can be estimated as:

$$\sigma^2 = \frac{\sum_{n=1}^{N} (s_n - \langle s \rangle)^2}{N-1}. \tag{9}$$

A commonly used rule of thumb [15] for the calculation of sampling lag is to set V equal to the sampling lag required for the autocorrelation function to become negative. The problem with this approach is that it is only based on linear statistics, and it does not account for any nonlinear dynamical correlation.

3.2 Time Delay Calculation: Mutual Information Method

The other method for the calculation of sampling delay is the using of *mutual information* function [5]. The original concept of mutual information is based on Shannon's information theory, which gives a measure of the general independence of two variables. In other words, this function provides the information about the signal at s_{n+V} given that we know s_n.

For a mathematical definition of this function, a histogram for the probability distribution of the signal is created. The probability that the signal has a value inside the ith bin of the histogram is denoted by p_i, and the probability that s_n is in bin i and s_{n+V} is in bin j is denoted by p_{ij}. Then the mutual information for sampling delay V can be defined as:

$$I(V) \;=\; \sum_{i,j} p_{ij}(V)\, \ln p_{ij}(V) \;-\; 2 \sum_{i} p_i \, \ln p_i. \tag{10}$$

It should be noted that the value of mutual information is independent of the choice of histogram, as long as it is fine enough. For large values of V, s_n and s_{n+V} have no correlation with each other; $p_{ij} = p_i \, p_j$ and the mutual information becomes zero.

The sampling lag related to the first minimum of mutual information function specifies the point where the information about s_{n+V} from knowledge of s_n is maximal, or where the redundancy is least. In general, the sampling lag value based on the autocorrelation function is not the same as the value from the mutual information function. In such cases, it is better to select an optimal V inside that interval. Optimal values of V can then be verified through the visualization of the data in a two-dimensional embedding.

3.3 Calculation of Optimal Sampling Delay for GKN Flight Data

The autocorrelation function of GKN time series data is shown in Figure 7. It should be noted that this function is periodic, and only part of the first period is shown. The optimal value of sampling delay based on this figure is between $V = 14$ and $V = 15$. For the final selection of the sampling delay, these results will be compared with the obtained value from mutual information function, and the final selection will be verified by visualizing the embedded data in the two-dimensional delay coordinates.

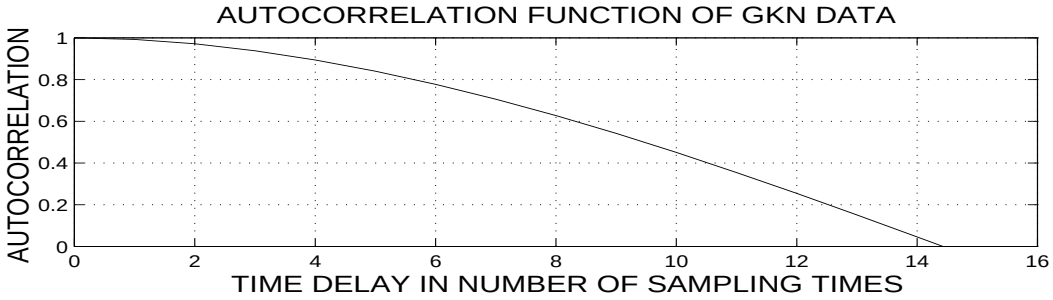

Figure 7: The autocorrelation function of GKN data

The mutual information of GKN data is illustrated in Figure 8. This function has a flat minimum around $V = 14$ to $V = 17$. Any value in this range should be a good choice for the sampling delay. Again, the final optimal sampling delay will be selected after inspecting the GKN data in two-dimensional delay coordinates.

Two-dimensional delay coordinate plots of the GKN time-series data are depicted in Figure 9 for six different values of sampling delay. As shown in this figure, for small values of V the points are projected along one diagonal. By increasing the value of V up to the range suggested by the autocorrelation and mutual information approaches, we obtain better projections in the two-dimensional coordinates. By increasing V beyond that range, all the points will be projected toward the other diagonal. From this visualization, the optimal value of $V = 15$ can be verified. It should be noted that other near-by values such as $V = 14$ and $V = 16$ also provide a good projection.

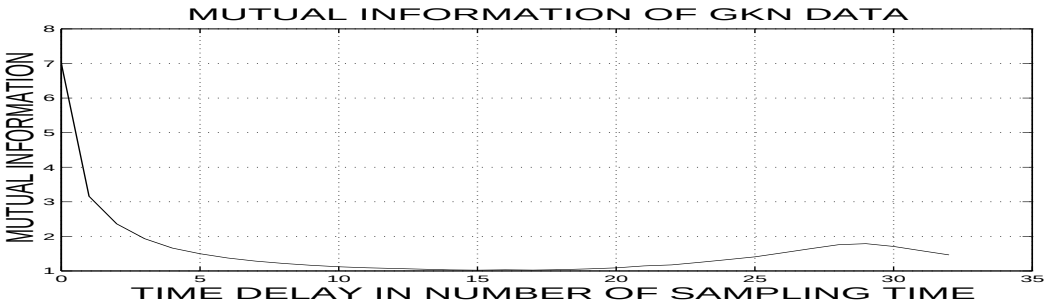

Figure 8: The mutual information function of GKN data

3.4 Calculation of Optimal Sampling Delay for Lorenz System

The mutual information of $x(t)$ variable from Lorenz System is shown in Figure 10. The first minimum of this function is around $V = 4$. This function is almost flat for higher values of V. The projection of the time series data of Lorenz System in a 2-dimensional embedding space for $V = 1$ to $V = 8$ is presented in Figure 11. By visualization of these plots, the optimal sampling delay of $V = 4$ is chosen.

4 Reconstructed State Space Embedding Dimension

As discussed in Section 2, the other important parameter for the state space reconstruction is the selection of embedding dimension. The embedding dimension, d, is the lowest integer dimension which unfolds the attractor in the projected space with no overlaps. Based on the embedding theorem [22], if the dimension of the attractor defined by the orbits in the original space is m, then the attractor can be unfolded in an integer dimensional space of dimension d where $d > 2m$. This condition is the sufficient dimension for the embedding, and in most cases a lower dimension can unfold the attractor. In other words, it can be guaranteed that a delay-coordinate with a higher dimension than $2m + 1$ is never necessary. The most common approach for the calculation of embedding dimension, d, is the *false nearest neighbours* approach [9], which is explained below.

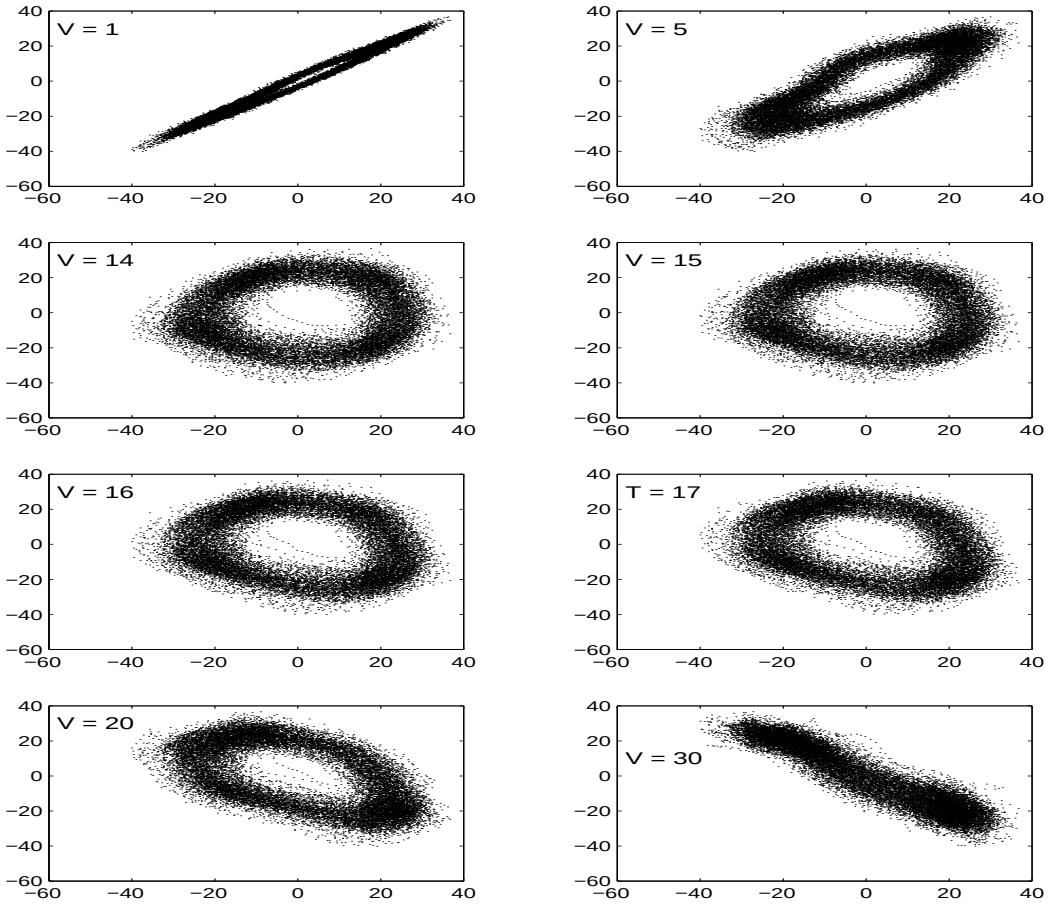

Figure 9: The two-dimensional embedding of GKN data for different sampling delays

4.1 Embedding Dimension: False Nearest Neighbors Method

For a d-dimensional delay-coordinate reconstruction of s_n (for $n = 1, 2, \cdots, N$), the delay vector at point k, $\mathbf{y}(k)$, can be written as:

$$\mathbf{y}(k) = [s_k, s_{k-V},\ \cdots,\ s_{k-(d-2)V},\ s_{k-(d-1)V}], \tag{11}$$

where V is found by the approach described in Section 3. The nearest neighbour of the vector $\mathbf{y}(k)$ is then determined, denoted by $\mathbf{y}^{NN}(k)$. In general, the vector $\mathbf{y}^{NN}(k)$ may be a true neighbour of $\mathbf{y}(k)$ due to its temporal nature, or it might be a false neighbour of $\mathbf{y}(k)$ due to projection from a higher dimension. In the former case, $\mathbf{y}^{NN}(k)$ is either the vector just behind or ahead of $\mathbf{y}(k)$ along its orbit. If the vector $\mathbf{y}^{NN}(k)$ is a false neighbour, the dimension d does not unfold the attractor, and going to a higher dimensions may move this false neighbour out of the neighbourhood of $\mathbf{y}(k)$. This procedure can be repeated for all the $\mathbf{y}(k)$ delay vectors, for $k = 1, 2, \cdots, N$. During this approach, the value of d is increased incrementally until no more false neighbours are removed. At this point d is equal to the embedding dimension of d, and the attractor is completely unfolded [9].

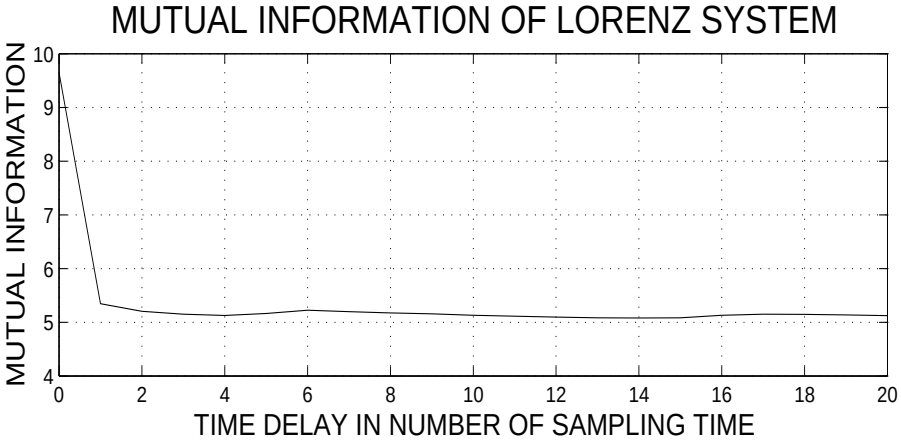

Figure 10: The mutual information function of $x(t)$ in the Lorenz System

In order to identify true and false neighbours, we use the Euclidean distance between the nearest neighbours in dimension d and $d+1$. In going to dimension $d+1$, the vectors $\mathbf{y}(k)$ and $\mathbf{y}^{NN}(k)$ are each augmented by s_{k-dV} and s^{NN}_{k-dV}, respectively. The Euclidean distance between the nearest neighbours in dimension d, denoted D_d, and in dimension $d+1$, D_{d+1}, can be formulated as:

$$D_d^2(k) \;=\; \sum_{i=1}^{d}[s_{k-(i-1)V} - s^{NN}_{k-(i-1)V}]^2 \tag{12}$$

$$D_{d+1}^2(k) \;=\; \sum_{i=1}^{d+1}[s_{k-(i-1)V} - s^{NN}_{k-(i-1)V}]^2 = D_d^2(k) + [s_{k-dV} - s^{NN}_{k-dV}]^2. \tag{13}$$

In fact, it is only necessary to compare the additional distance $|s_{k-dV} - s^{NN}_{k-dV}|$ with $D_d^2(k)$, the Euclidean distance in dimension d. If the additional distance in comparison to the distance of nearest neighbours in dimension d is large, the neighbours are false; otherwise, the neighbours are true. The normalized distance difference in dimension d and $d+1$ with respect to the distance in dimension d, ΔD_d, can be written as:

$$\Delta D_d(k) \;=\; \frac{|s_{k-dV} - s^{NN}_{k-dV}|}{D_d(k)}. \tag{14}$$

Whenever the value of ΔD_d is greater than some predefined threshold, the neighbours are declared to be false. The value of this threshold is very important in declaring false neighbours. In general, the threshold value depends on the application, and it varies with the noise level and the number of data points. In general, if all regions of the attractor are sampled adequately, the variation of false neighbours with the number of data points is very small.

The false nearest neighbours method is very effective as long as the time series data are not corrupted by noise. In fact, for clean time series data the number of false nearest

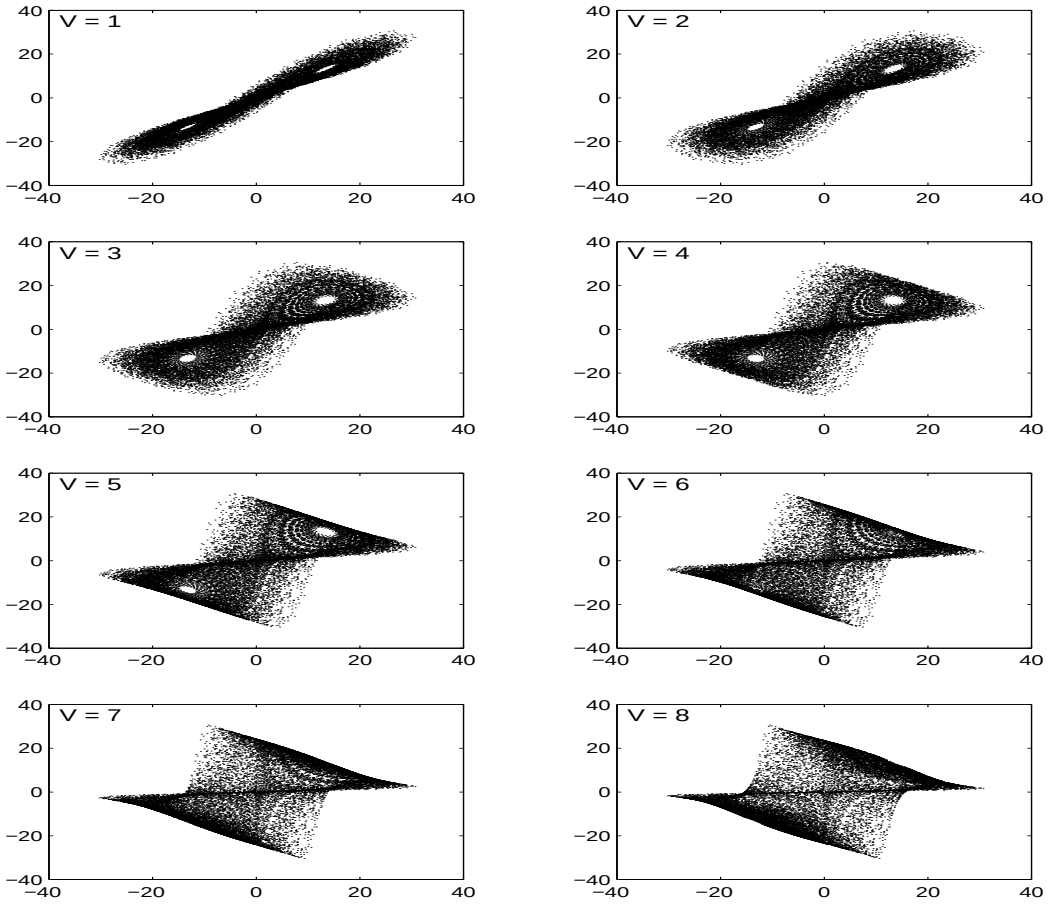

Figure 11: The two-dimensional embedding of $x(t)$ in the Lorenz System for different sampling delays

neighbours drops to zero as d approaches the embedding dimension. By increasing the delay-coordinate dimension beyond that point, the false nearest neighbours stay equal to zero, since after the attractor is unfolded for d, it stays unfolded for any dimension greater than d. In real-life applications, the time series data are always contaminated by noise, and in some cases the noise may dominate the signal. In such conditions, the embedding dimension would be increased until the noise is also unfolded. As we know, the dimension of noise is very high. As a result, by increasing the value of d, the false nearest neighbours may never drop near to zero. In these cases, when the false nearest neighbours value comes to its minimum, we can stop increasing the value of d. If the noise level is not very high, it is also possible to put the threshold value of false nearest neighbours greater than noise level [9].

4.2 Dimension Calculation of Reconstructed State Space for GKN Data

The false nearest neighbours algorithm is used to calculate the delay-coordinate dimension of the GKN time series data. The result of this calculation is presented in Figure 12. As shown in this figure, the value of false nearest neighbours is very close to zero for $d = 6$. This value will be selected for delay-coordinate state space reconstruction of GKN data.

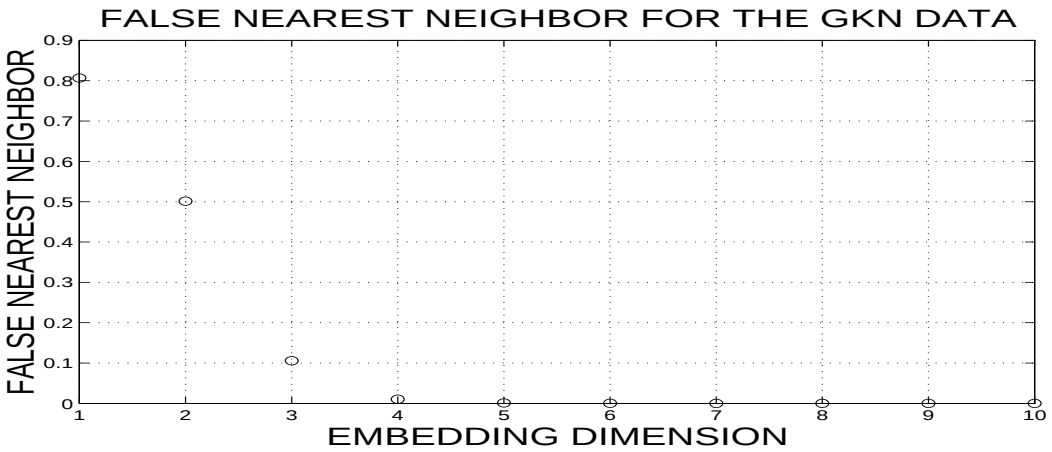

Figure 12: Calculation of embedding dimension of GKN data by false nearest neighbours approach

4.3 Dimension Calculation of Reconstructed State Space for Lorenz System

The delay-coordinate dimension of Lorenz System is also calculated by using the false nearest neighbours approach. Based on these results, a value of $d = 3$ can unfold the Lorenz System.This value is equal to the actual dimension of system, $m = 3$. In the following analysis, the value of $d = 3$ is used as the mimimum embedding dimension of Lorenz System.

5 Lyapunov Exponents

In general, the trajectory of a dynamical system starting at an arbitrary initial point can end up at a stable fixed point (sink), a stable closed trajectory (periodic sink), a chaotic orbit, or it may become unstable (see Appendix A). The evolution of such a trajectory may be quite complicated, for example, if an initial condition is near an

unstable fixed point (source) p, it experiences an unstable behaviour in the beginning – the distance between the orbit points and the source increases at an exponential rate. In a one-dimensional map, F, this distance is multiplied by $|F'(p)| > 1$ at each iteration. At some distance from the source, the orbit may be attracted to a sink q. Near the sink, the distance between the orbit points and the sink will reduce by the factor $|F'(p)| < 1$. This transient instability and attraction to a sink or period-K sink is not generic in all dynamical systems; in some systems, there may be no stable solutions or there may be chaotic orbits.

A chaotic orbit can be defined as continuously unstable behaviour of the system. Here the term "unstable" is not used to mean that the orbit completely diverges, as is the case for unstable fixed points or unstable closed trajectories (limit cycles); rather, in such a system, initial points near the orbit are not attracted to any sink yet the signals do not become arbitrarily large. At any point of such an orbit, there are points arbitrary near, that will move away from each other during further iterations. This behaviour is in marked contrast to that of a stable limit cycle, where nearby points converge. To discriminate between these phenomena (stable limit cycles and chaotic orbits), the Lyapunov number (or Lyapunov exponent) can give us a useful measure of the convergence or divergence (chaotic behaviour) of the system's orbits. The Lyapunov number is defined as the average per-step divergence rate of nearby points along a system's orbits, and the Lyapunov exponent is the natural logarithm of the Lyapunov number.

5.1 Lyapunov Number/Exponent in One-Dimensional Maps

As outlined in Appendix A, the stability of a discrete dynamical system around any fixed point is governed by the derivative of its map. For example, in a one-dimensional map F with fixed point p and $F'(p) > 1$, the orbit of any point x near p will diverge from p at a multiplicative rate of approximately $F'(p)$ per iteration. Similarly, for a period-K orbit, the derivative of the Kth iterate of the map determines the behaviour of the map. This derivative, according to the chain rule, is equal to the product of the map's derivatives at the K points of the orbit. In this case, the orbit of each point x close to the periodic point p_K, after each K iterations, converges to or diverges from p_K at a rate about equal to the product of the derivatives.

The Lyapunov number is defined to quantify the average convergence or divergence of near-by points at each iteration. A Lyapunov number of 2 (or Lyapunov exponent of $\ln 2$) means that the average distance between the orbit of x_1 and the orbit of a neighbouring point x_1' doubles each iteration. If the Lyapunov number is less than one, e.g. $\frac{1}{2}$, then the distance would be halved at each iteration, and points x_1 and x_1' become closer. For a period K orbits p_K, this measure can be formulated as:

$$|(F^K)'(p_K)| \;=\; |F'(x_1)|\,|F'(x_2)|\,...\,|F'(x_K)| \tag{15}$$

To formalize this discussion, the sensitive dependence of chaotic systems on initial conditions can be distinguished from the behaviour of stable limit cycles (period-K sinks) by the Lyapunov number or exponent; clearly, these are the only two options given a vibratory signal that does not diverge in the traditional sense of instability. In fact, an orbit is chaotic if its Lyapunov number is greater than 1. In mathematical form, the Lyapunov number and exponent can be defined as follows:

Lyapunov number: Let F be a one-dimensional map on $\Re$. The Lyapunov number, $L(x_1)$, of the trajectory $\{x_1,\ x_2,\ x_3,\ \cdots\}$ is defined as:

$$L(x_1) \ = \ \lim_{n\to\infty} \left(|F'(x_1)|\ |F'(x_2)|\ ...\ |F'(x_n)|\right)^{1/n} \tag{16}$$

if this limit exists.

Lyapunov exponent: The Lyapunov exponent, $\lambda(x_1)$, exists if and only if L exists, and can be defined similarly as:

$$\lambda(x_1) \ = \ \ln L \ = \lim_{n\to\infty} (1/n)\ [\ \ln(|F'(x_1)| + \ln|F'(x_2)| + ... + \ln|F'(x_n)|\ ]. \tag{17}$$

It should be noted that the Lyapunov number/exponent cannot be defined for any trajectory containing a point x_i with $F'(x_i) = 0$. For a one-dimensional map F, the Lyapunov number/exponent of a fixed point p is:

$$L \ = \ |F'(p)|; \qquad \lambda \ = \ \ln|F'(p)|, \tag{18}$$

and for period-K point p_K, the Lyapunov number and exponent are:

$$L(p_K) \ = \ \left(|F'(x_1)||F'(x_2)|...|F'(x_K)|\right)^{1/K}. \tag{19}$$

$$\lambda(p_K) \ = \ \left(\ln|F'(x_1)| + \ln|F'(x_2)| + ... + \ln|F'(x_K)|\right) / K. \tag{20}$$

The unit of Lyapunov exponent is in inverse normalized time, and it provides a measure of the rate of divergence or convergence of nearby trajectories with each time step. In calculating the Lyapunov exponent, the time unit can be equal to the unit of the sampling time index or the unit of real time, say seconds [2].

5.2 Lyapunov Numbers and Exponents for Multidimensional Maps

Lyapunov numbers and exponents can also be defined for multidimensional maps. In a one-dimensional map, a single Lyapunov number gives a measure of separation rates of nearby points along the real line. For maps on $\Re^m$ for $m > 1$, however, nearby points may diverge in one direction and converge in another. Therefore, in an m-dimensional map, each orbit has m Lyapunov numbers. These numbers measure

the rate of expansion/contraction from the current point along m orthogonal directions. In general, the *maximal* Lyapunov number/exponent is the most important one for identifying chaotic behaviour of a system, since divergence (a positive Lyapunov exponent) in some direction(s) is a signature for chaos.

As an example, consider a 2-dimensional map with expansion on one direction and contraction on the other axis. Take a circle with infinitesimal radius centered on the first point $\mathbf{x}_0$ of the orbit. After each iteration of map $\mathbf{F}$ on the points inside this small disk, the points on the circle are expanded along one direction, and contracted on the other direction. This causes the small circle to change into an ellipse. After each iteration of mapping, the ellipse becomes longer and thinner. The result of this mapping for a unit circle after n iteration is shown in Figure 13. The expansion/contraction of the axes of the ellipse at each iteration is governed by the Lyapunov numbers. The natural logarithm of each Lyapunov number is the corresponding Lyapunov exponent.

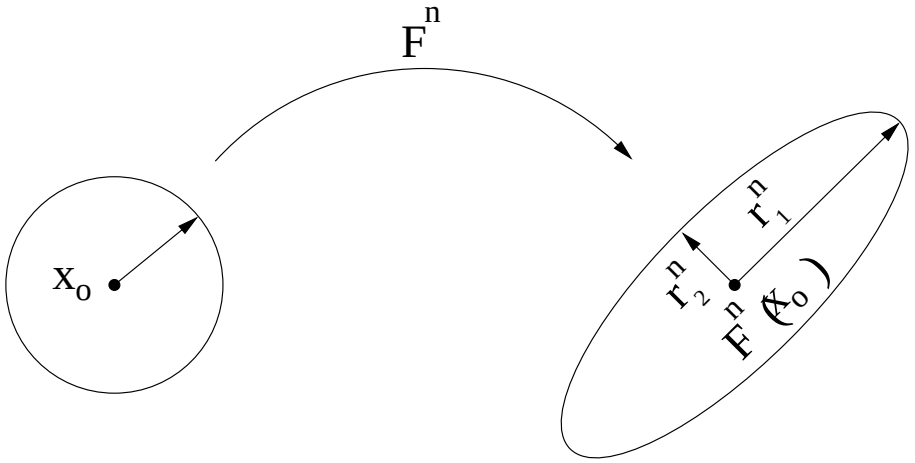

Figure 13: Effect of expansion and contraction in a 2-dimensional map

In order to define the Lyapunov number in a multidimensional map, let the Jacobian (the first derivative matrix) of $\mathbf{F}$ at $\mathbf{x}_0$ be denoted by $\mathbf{J}_0 = \mathbf{DF}(\mathbf{x}_0)$, and the Jacobian of the nth iterate of $\mathbf{F}$ at $\mathbf{x}_0$ by $\mathbf{J}^n = \mathbf{DF}^n(\mathbf{x}_0)$ In the multidimensional case $m > 2$, the circle and ellipse are replaced by hypersphere and hyperellipsoid. Since we are considering the infinitesimal behaviour of map $\mathbf{F}$ around $\mathbf{x}_0$, the map can be replaced by its linearized model at $\mathbf{x}_0$, $\mathbf{x}_{n+1} = \mathbf{J}_0\mathbf{x}_n$. For simplicity, the small sphere is also replaced by the unit sphere U. As a result, $\mathbf{J}_0 U$ determines the ellipsoid with m orthogonal axes after the first iteration, and $\mathbf{J}^n U$ will be the ellipsoid after n iterations. The Lyapunov number can now be defined as follows:

Lyapunov number: Let $\mathbf{F}$ be a smooth map on $\Re^m$, and for $k = 1, \cdots, m$, let r_k^n be the length of the kth longest orthogonal axis of the ellipsoid $\mathbf{J}^n U$ for an orbit with initial point $\mathbf{x}_0$. Then r_k^n gives the expansion or contraction near the orbit of $\mathbf{x}_0$ during the first n iterations. The kth Lyapunov number of $\mathbf{x}_0$ is defined by:

$$L_k = \lim_{n\to\infty} (r_k^n)^{1/n}, \tag{21}$$

if the limit exists.

Lyapunov exponent: With the similar notation, the kth Lyapunov exponent of $\mathbf{x}_0$ can be defined as:

$$\lambda_k \;=\; \ln L_k \;=\; \ln(\lim_{n\to\infty}(r_k^n)^{1/n}). \tag{22}$$

It should be noted that in these definitions, it is given that $L_1 \geq L_2 \geq \cdots \geq L_m$ and $\lambda_1 \geq \lambda_2 \geq \cdots \geq \lambda_m$.

According to the definitions above of Lyapunov number/exponent, a chaotic orbit in a multidimensional map can be defined as follows:

Chaotic orbit: Let $\mathbf{F}$ be a map of $\Re^m$, $m \geq 1$, and let $\mathbf{x}_0, \mathbf{x}_1, \mathbf{x}_2, \cdots$ be a bounded orbit of $\mathbf{F}$. The orbit is chaotic if:

1. it is not asymptotically periodic,
2. no Lyapunov number (exponent) is exactly one (zero), and
3. $L_1(\mathbf{x}_0) > 1$ ($\lambda_1(\mathbf{x}_0) > 0$).

In a chaotic system, the separation of nearby trajectories may be extremely fast. The average maximal rate of this divergence, characterized by the maximal Lyapunov exponent, characterizes the strength of the chaos. If the separation rate is averaged over a short time, we obtain a *local Lyapunov exponent*. Local Lyapunov exponents can have strong fluctuations [18], and are difficult to interpret. The (global) Lyapunov exponent is an average over the local values, and tends to be more consistent.

Again, the maximal Lyapunov exponent, λ_1, is the most important. From the value of λ_1 for a particular trajectory, we can determine if the system has a stable fixed point, a stable limit cycle, or if it exhibits chaotic behaviour. Dissipative systems have a negative maximal Lyapunov exponent, and separate trajectories are attracted to a stable fixed point. These trajectories approach each other exponentially fast when they are approaching the stable fixed point. If the system has a stable limit cycle, two separate trajectories can approach each other exponentially ($\lambda_1 < 0$) or more slowly than exponentially ($\lambda_1 = 0$). In a chaotic system, the maximal Lyapunov exponent is positive, $\lambda_1 > 0$. In this case, the nearby trajectories diverge from each other exponentially fast. Note that for a random noise, the maximal Lyapunov exponent is infinite. The summary of the system behaviour and its relation with Lyapunov exponent is shown in Table 1 [8].

It should be mentioned that the Lyapunov exponent is an *invariant* of the system. In numerical calculation of Lyapunov exponents from time series data, as long as the data has enough resolution, the type of measurement, sampling time, or use of a smooth transformation does not change the resulting values of the Lyapunov exponents. In calculating Lyapunov exponents using the delay-coordinate embedding approach, the

Table 1: Relation of Maximal Lyapunov Exponent and System Behaviour

Type of motion	Maximal Lyapunov exponent
stable fixed point	$\lambda_1 < 0$
stable limit cycle	$\lambda_1 \leq 0$
chaos	$0 < \lambda_1 < \infty$
noise	$\lambda_1 = \infty$

local Lyapunov exponent varies throughout the attractor, and the actual exponent is an appropriate average over the whole space.

5.3 Measuring the Maximal Lyapunov Exponent from Time Series Data

As mentioned, the maximal Lyapunov exponent is of paramount importance. For this reason, most algorithms used in the study of chaos deal with the calculation of this exponent. In this section, an algorithm which calculates the maximal Lyapunov exponent from time series data is discussed [7, 17]. In this algorithm, the exponential divergence of nearby trajectories is tested. Thus, for data with no finite exponent, such as noise, no Lyapunov exponent will be calculated.

Recall that the (global) Lyapunov exponent is an average over the local Lyapunov exponent in the whole attractor space. In another words, the Lyapunov exponent is the average of exponential expansion/contraction rates over the whole time series data. In most cases, the time series data are contaminated by noise. In order to reduce the effect of noise on the calculation of the Lyapunov exponent, some appropriate averaging (filtering) method should be deployed.

The Lyapunov exponent can be calculated using the delay-coordinate embedding approach as follows:

1. Select a reference point s_{k_0} from the time series data and identify $\mathbf{y}_{k_0} = \mathbf{y}(k_0)$ in the delay-coordinate embedding space as:

$$\mathbf{y}_{k_0} = [s_{k_0}, s_{k_0-V},\ \cdots,\ s_{k_0-(d-2)V},\ s_{k_0-(d-1)V}] \tag{23}$$

   where the values of V and d are calculated as discussed in Sections 3 and 4, respectively.

2. Find all the points in the neighbourhood of $\mathbf{y}_{k_0}$ with the distance smaller than ϵ, $\mathcal{U}_\epsilon(\mathbf{y}_{k_0})$.

3. Calculate $D(0)$, the average of distances between $\mathbf{y}_{k_0}$ and the points in $\mathcal{U}_\epsilon(\mathbf{y}_{k_0})$.

4. Calculate $D(\Delta k)$, the average of the same distances after Δk time steps, for $\Delta k = 1, 2, \ldots$.

5. Calculate the logarithm of the calculated values of Item 4, and get its average over all the data points.

6. Plot the calculated values of Item 5, $D_l(\Delta k)$, versus Δk. The slope of this graph is the Lyapunov exponent per time step. This value can be converted to the normal time unit.

In general, the embedding dimension and time lag of the delay-coordinate may not be known *a priori*. In these cases, several values for each one can be examined. The selected value of ϵ should be as small as possible, but it should be large enough that each point has at least several neighbours. This causes all the parts of the attractor to participate in the calculation, and thus a better value of the Lyapunov exponent is obtained.

In order to minimize computational effort, it is possible to reduce the number of data points used during the above calculations. One option is to stop the computation as soon as a sufficient number of reference points with rich neighbourhoods are obtained. The minimum number of reference points can be as low as 500 points, and the number of neighbours for each reference point should be greater than 10 [8]. In general, reference points with fewer neighbours will cause more fluctuation in the value of D_l. Fluctuations in D_l can also occur due to the presence of noise in the data set. If the noise level is bigger than ϵ, some false neighbours may be considered as true neighbours, and the value of D_l thereby corrupted.

5.4 Calculation of the Maximal Lyapunov Exponent for GKN Data

PRELIMINARY RESULTS

The GKN data set is studied by using the method explained in Section 5.3. The sampling delay of $V = 14$, and the minimum dimension of $d = 6$ are selected. The value of $D_l(\Delta k)$ is calculated by the methods mentioned in [7] and [17]. The following results were obtained using software supplied by the authors [7, 17].

In the approach followed from [7], the value of $D_l(\Delta k)$ is calculated for neighbourhood sizes of $\epsilon = 6$ and $\epsilon = 8$, and five different dimensions $d = 6, 7, \cdots, 10$, resulting in 10 cases. The selected number of reference points is equal to 1000, and the number of points in the ϵ-neighbourhood of reference points with the selected ϵ was from 50 to 1000. All the plots are presented in Figure 14.

In this figure, we note that a similar behaviour is obtained in each case. The initial strong fluctuation of D_l are due to the presence of quasiperiodicity in the dynami-

cal system. Underlying these fluctuations, a distinct linear increase is apparent, as shown by the dashed line. The slope of this line gives the estimated value of the maximal Lyapunov exponent. The calculated value of maximal Lyapunov exponent from Figure 14 is $\lambda_1 = 2.99 * 10^{-3}$ 1/time step or $\lambda_1 = 3.07$ 1/second.

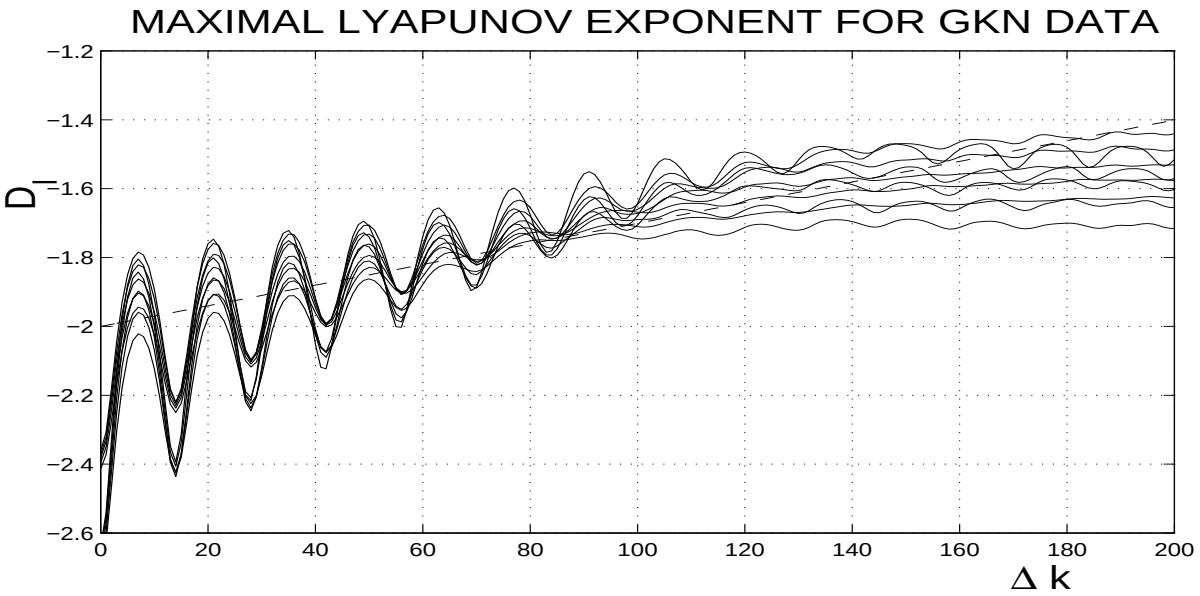

Figure 14: Maximal Lyapunov exponent calculation for the GKN data by the method of [7]

The maximum Lyapunov exponent is also calculated by the approach mentioned in [17]. In this method, the value of ϵ is automatically changed until enough number of neighbors are found, the dimension values of $d = 6,\ 10,\ 14,\ 18$ are examined. The obtained plots from this method with the dashed line with the same slope are illustrated in Figure 15. In this figure, the plot for $d = 6$ has the same linear increase as mentioned above, and the slope of the other plots will decrease when the value of d increases. This drop could be due to the corruption of the data with noise. As mentioned in [8], the noise can have major impacts on the computation of Lyapunov exponent. For the calculation of Lyapunov exponent more accurately, the measured data should be filtered very precisely. Many linear and nonlinear filtering algorithms for chaotic data are proposed in the literature. The selection of the appropriate algorithm is another important issue.

For considering the effect of sampling delay on the computed Lyapunov exponent, for the dimension of $d = 6$ several different values of sampling delays, $V = 10,\ 11,\ 12,\ 14,\ 16,$ and 18 are tested. The results of this case by the method of [17] are shown in Figure 16. In all the plots, the dashed line has a slope equal to the mentioned value. As it is clear from these plots, the change of V by only one or two does not have much impact on λ_1, but larger values can have some effects on the computed value of λ_1. It should be noted that in real-life time series, the number of data points and sampling time can

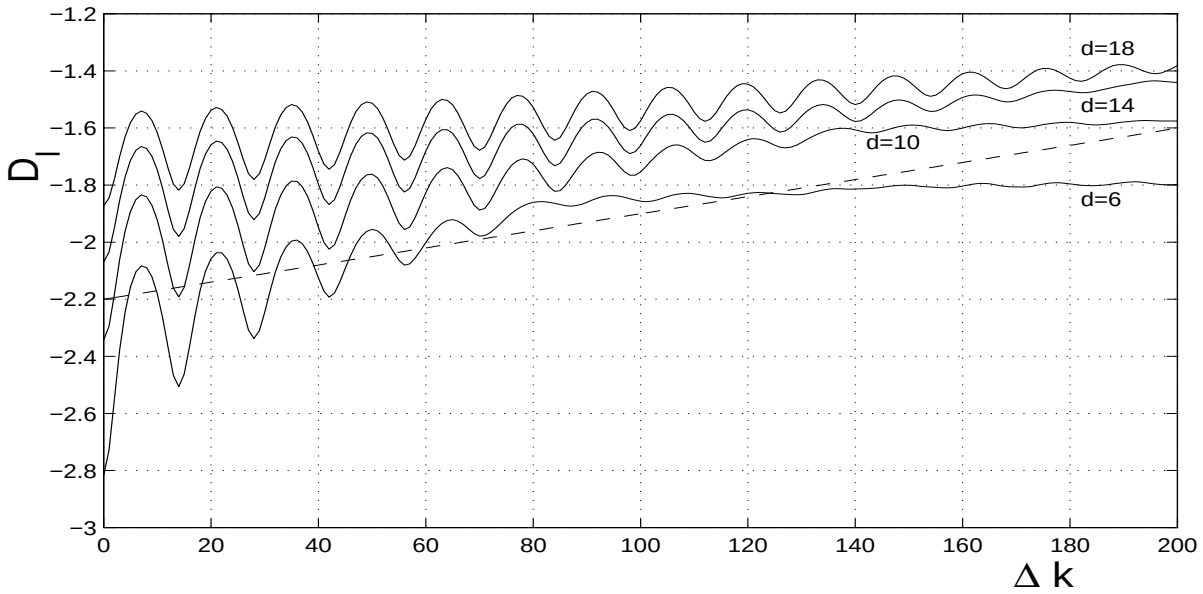

Figure 15: Maximal Lyapunov exponent calculation for the GKN data by the method of [17]

also have some effects on the computed Lyapunov exponent. For the consideration of this case, a new data set by removing every other point of the original data is created. By using the same approaches, the new optimal sampling delay, V, and embedding dimension are estimated. The plots for the new data set for four different values of dimension, $d = 6,\ 10,\ 14,$ and 18 from the approach of [17] are presented in Figure 17. The dashed line has the slope of $\lambda_1 = 5.98E - 3$ 1/time step or 3.06 1/second. From this figure, it can be concluded that the sampling time can have small effect on the calculated value of λ_1.

5.5 Calculation of the Maximal Lyapunov Exponent for Hénon Map and Lorenz System

For verification of our analysis in the computation of λ_1, two classical example are also examined. As an example of a discrete system, the value of λ_1 for Hénon Map by the approach of [7] is calculated. The plots of D_l for this map for $d = 2, 3, 4$, and several values of ϵ is shown in Figure 18. The expected value of λ_1 as reported in the literature [17] is equal to 0.418. The slope of this line in Figure 18 is shown by the dashed line. As can be seen, the slope of D_l for different values of d and ϵ is very close to the slope of the dashed line.

The maximal Lyapunov Exponent of $x(t)$ and $z(t)$ of Lorenz System is also computed by using the approach of [7]. The value of D_l is calculated for $d = 3, 4, 5, 6$, and several values of ϵ. All the plots for $x(t)$ and $z(t)$ are illustrated in Figure 19 and 20,

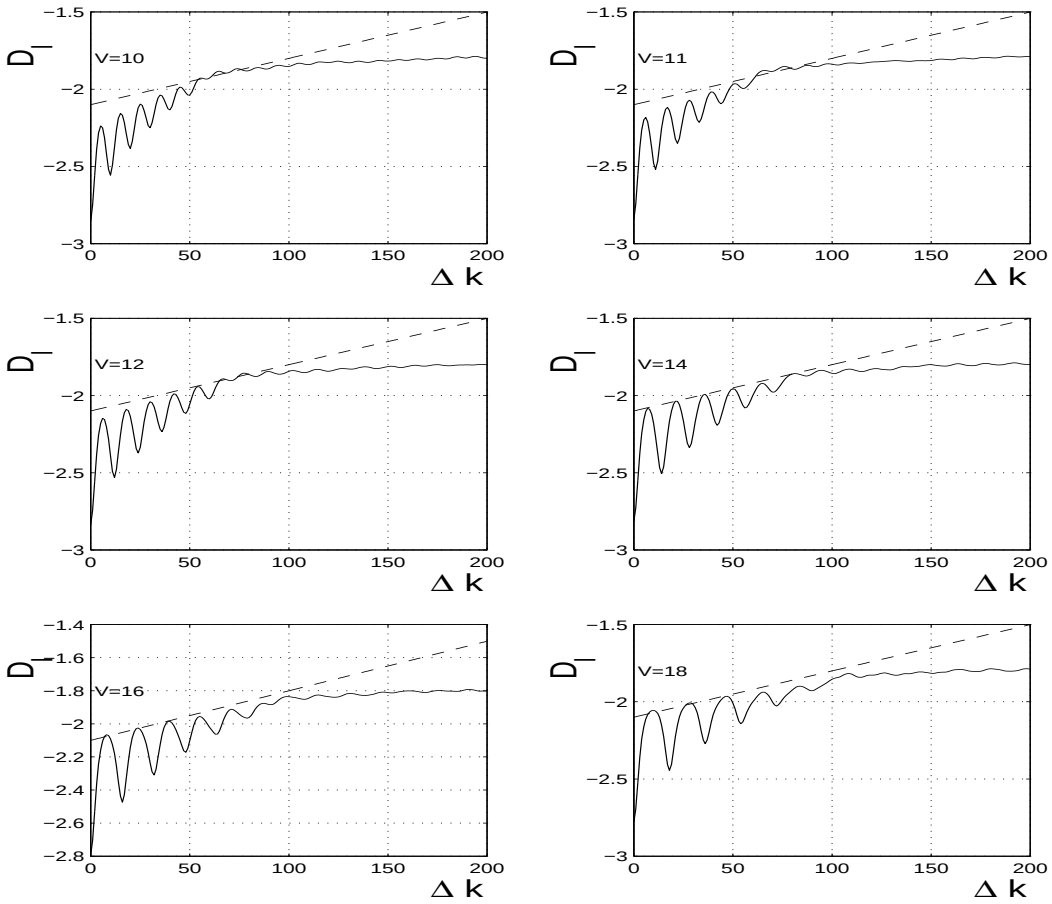

Figure 16: The effect of reconstruction sampling delay on maximal Lyapunov exponent computation for $d = 6$

respectively. The dashed line in Figure 19 has a slope equal to the expected value of $\lambda_1 = 1.5$ [17]. As it is clear, the slope of D_l is in accordance with the reported value in the literature. The dashed line in plots of Figure 20 has a slope equal to $\lambda_1 = 1.14$. We have not found any reported value for this Lyapunov Exponent, and no comparison can be made. The fluctuation of D_l in these figure are related to the values of $d > 3$ and small values of ϵ.

6 Conclusion

A preliminary analysis of flight data from the GKN EH101 Helicopter has been performed in order to investigate the possibility of chaotic behaviour. The motivation of this study is to find the vibrational characteristics of a helicopter during flight, and to determine the best way to reduce these vibrations. Two sets of flight data related to the acceleration of helicopter for different airspeeds were considered. The data were

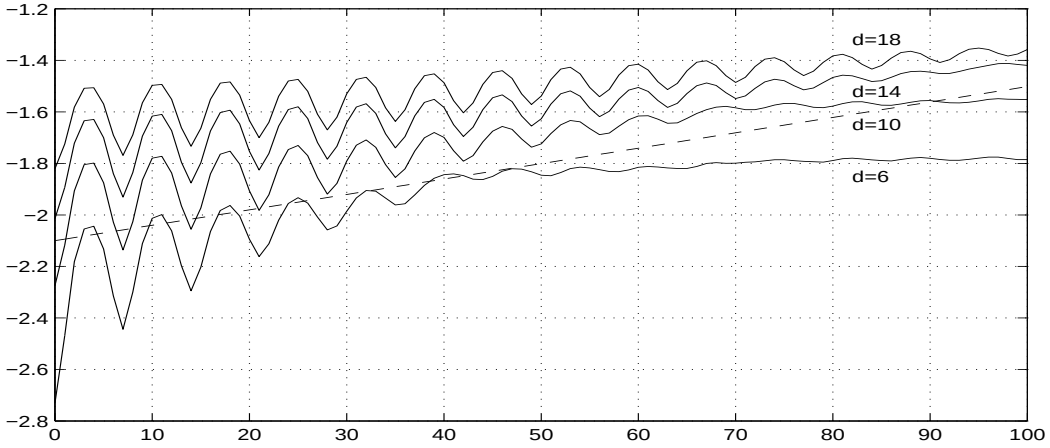

Figure 17: Maximal Lyapunov exponent computation for half of the GKN data

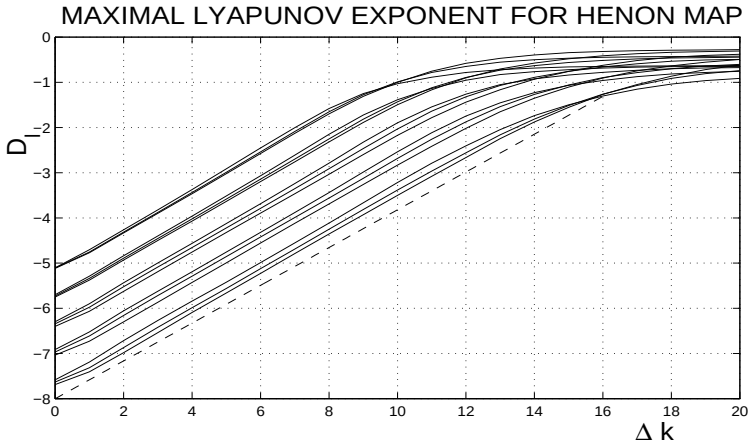

Figure 18: Maximal Lyapunov exponent calculation of Hénon Map by the approach of [7]

sampled at f_s=1024 Hz at the nominal rotor speed of $f_n = 3.57$ Hz, when the active vibration control of helicopter is switched off.

As a first step, the time series data was inspected in the frequency domain. The blade passing frequency of $5f_n$=17.85 Hz has the highest amplitude in the power spectrum of the data; however, significant power over a broad range of frequencies is also present. The general sources of broad band frequency content can be random noise or chaos. For this reason, the presence of chaos in the time series data may be suspected.

One of the major characteristics of chaotic systems is their sensitive dependence of their trajectory to the initial conditions. Two trajectories with very close initial conditions can move apart completely. This characteristic can be quantified by the Lyapunov exponent; in particular, chaotic systems have a maximal Lyapunov ex-

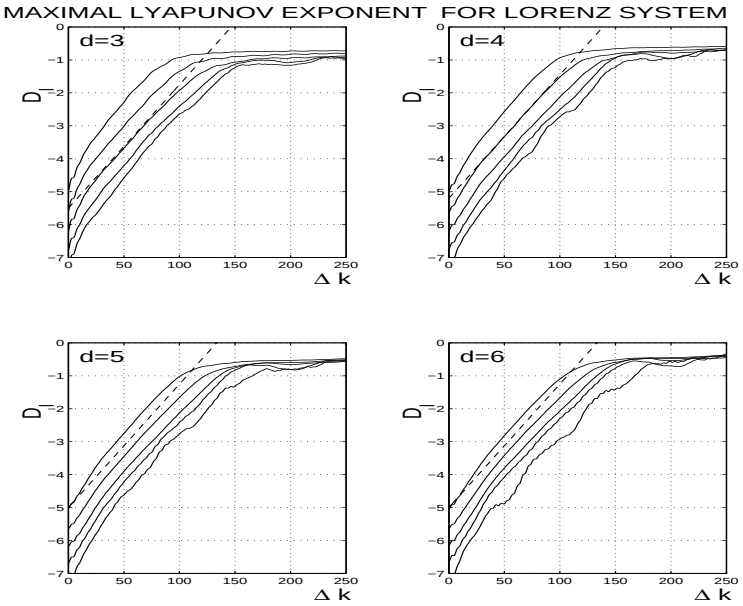

Figure 19: Maximal Lyapunov exponent calculation of $x(t)$ in the Lorenz System by the approach of [7]

ponent greater than zero. In order to calculate the Lyapunov exponent, the given time series data were used to reconstruct a state space representation. The delay-coordinate embedding approach was used for this purpose. The selection of sampling delay and dimension of the embedding space were the main considerations; these are thoroughly discussed.

The optimal sampling delay for the GKN time series data was calculated using the autocorrelation and mutual information functions. The final selection was verified by inspecting the data embedded in a 2-dimensional delay-coordinate state space. The dimension of the GKN data was computed by the false nearest neighbours approach. These parts of the analysis are well understood and appear to have produced significant new understanding and results.

The Lyapunov exponent of the embedded system was calculated by two of the methods proposed in the literature and using software supplied by the authors. The maximum Lyapunov exponent derived from the GKN data was equal to $\lambda_1 = 2.99 * 10^{-3}$ 1/time step or $\lambda_1 = 3.07$ 1/second. This value is greater than zero, and shows the exponential divergence of nearby points. As a result, the system appears to have a chaotic behaviour. This work is still considered speculative, and further study, including methods of noise reduction, is planned.

The control of chaos in dynamical system is discussed considerably in the literature. Before any study for the control of this system can be contemplated, however, further study and analyses are recommended.

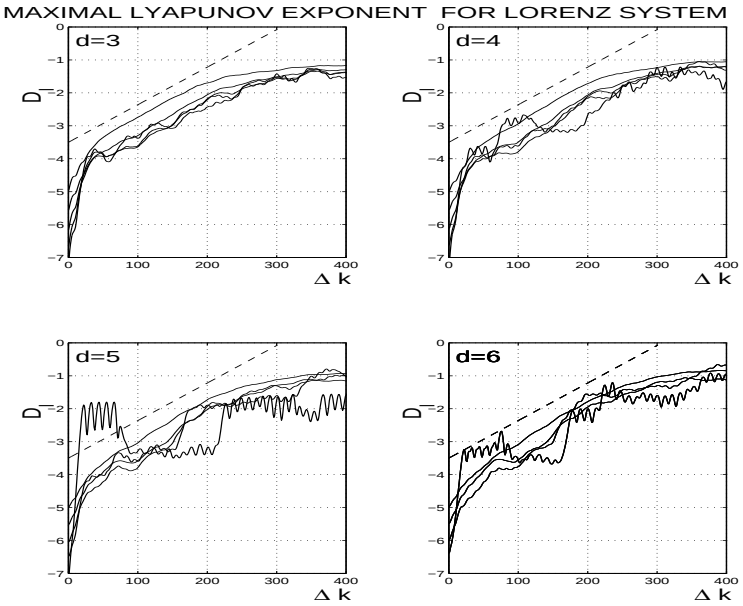

Figure 20: Maximal Lyapunov exponent calculation of $z(t)$ in the Lorenz System by the approach of [7]

7 References

[1] H. D. I. Abarbanel, *Analysis of Observed Chaotic Data*, Springer, 1996.

[2] K. T. Alligood, T. D. Sauer, J. A. Yorke, *An Introduction to Dynamical Systems*, New York: Springer-Verlag, 1997.

[3] Casdagli, M., "Chaos and deterministic versus stochastic nonlinear modeling" *Journal of the Royal Statistical Society B*, 54, 1991, pp. 303

[4] Casdagli, M. , Eubank, S., Farmer, J. D., Gibson, J. "State space reconstruction in the presence of noise" *Physica D*, 51, 1991, pp. 52.

[5] A. M. Fraser, H. L. Swinney, "Independent coordinates for strange attractors from mutual information", *Physical Review A*, 33, 1986, pp. 1134.

[6] S. Hayes, C. Grebogi, E. Ott, "Communicating with chaos" *Physical Review Letters*, 70/3031, 1993, pp. 3031.

[7] H. Kantz "A robust method to estimate the maximal Lyapunov exponent of a time series", *Physical Review A*, 185, 1994, pp. 77.

[8] *Nonlinear time series analysis*, by Holger Kantz, Maz Planck Institute for Physics of Complex Systems, Dresden Thomas Schreiber, Physics Department, University of Wuppertal, 1997.

[9] M. B. Kennel, R. Brown, and H. D. I. Abarbanel, "Determining embedding dimension for phase-space reconstruction using a geometrical construction", *Physical Review A*, 45, 1992, pp. 3403.

[10] D. Kugiumtzis, B. Lillekjendlie, N. Christophersen, "Chaotic time series I", *Modeling, Identification and Control*, 15, 1994, pp. 205.

[11] W. Liebert, H. Schuster, "Proper choice of the time delay for the analysis of chaotic time series" *Physical Review A*, 142, 1989, pp. 107.

[12] A. I. Mees, P. E. Rapp, L. S. Jennings, " Singular-value decomposition and embedding dimension", *Physical Review A*, 36, 1987, pp.340.

[13] E. Ott , C. Grebogi, J. A. Yorke, "Controlling chaos, controlling chaotic dynamical systems" *Physical Review Letters*, Volume 64, 1996, pp. 153-172; also in CHAOS/XAOC, American Physical Society, edited by D. Campbell, 1990, pp. 77-80.

[14] E. Ott, *Chaos in Dynamical Systems*, Cambridge University Press, 1993.

[15] E. Ott, T. Sauer, J. A. Yorke, *Coping with Chaos: Analysis of Chaotic Data and the Exploitation of Chaotic systems*, New York, Wiley, 1994.

[16] N. Packard, J. Crutchfield, J. D. Farmer, R. Shaw, "Geometry from a time series", *American Physical Society*, 1980, pp. 712-715.

[17] M. T. Rosenstein, J. J. Collins, C. J. De Luca, "A practical method for calculating largest Lyapunov exponents from small data sets", *Physica D*, 65, 1993, pp. 117.

[18] M. Sano and Y. Sawada, "Measurement of the Lyapunov spectrum from a chaotic time series", *Physical Review Letters*, Volume 55, 1985, pp. 1082-1085

[19] M. Sano and Y. Sawada, "Measurement of the Lyapunov spectrum from a chaotic time series", *Physical Review Letters*, 55, 1985, pp. 1082.

[20] T. Sauer, J. Yorke, and M. Casdagli, "Embedology", *Journal of Statistical Physics*, 65, 1991, 579.

[21] Nonlinear Modeling, Advanced Black-Box Techniques, Edited by Johan A. K. Suykens, and Joos Vanderwalle, 1998.

[22] F. Takens, "Detecting strange attractors in turbulence", in *Dynamical Systems and Turbulence*, Edited by D. A. Rand and L.-S. Young, Warwick 1980.

Appendix A: Definitions

Attracting Fixed Point: Let F be a map on $\Re$ and let p be a real number such that $F(p) = p$. If all points sufficiently close to p are attracted to p, then p is called an attracting fixed point or sink. In other words, if there is an $\epsilon > 0$ such that for all x in the $\epsilon - neighbourhood$ of p, $\mathcal{U}_\epsilon(p)$, $\lim_{k\to\infty} F^k(x) = p$, then p is a sink. For a smooth map on $\Re$ with the fixed point of p, if $|F'(p)| < 1$, then p is a sink.

In multidimensional case, let $\mathbf{F}$ be a map on $\Re^m$, and let $\mathbf{p}$ be in $\Re^m$ such that $\mathbf{F}(\mathbf{p}) = \mathbf{p}$. If there is an $\epsilon > 0$ such that for all $\mathbf{v}$ in the ϵ-neighbourhood of $\mathbf{p}$, $\mathcal{U}_\epsilon(\mathbf{p})$, $\lim_{k\to\infty} \mathbf{F}^k(\mathbf{v}) = \mathbf{p}$, then $\mathbf{p}$ is an attractor or sink. If the magnitude of each eigenvalue of $\mathbf{DF}(\mathbf{p})$ (see Jacobian matrix) is less than 1, then $\mathbf{p}$ is a sink.

Attractor: An attractor in a multi-dimensional state space is the set of points which solves the equation of a dynamical system after transients have damped out. An attractor with an integer dimension is called a *regular attractor*, and with a fractional dimension is termed as a *strange attractor*.

Basins of Attraction: Let $\mathbf{F}$ be a map on $\Re^m$ and $\mathbf{p}$ be an attracting fixed point or periodic point for $\mathbf{F}$. The basin of attraction of $\mathbf{p}$, or just basin of $\mathbf{p}$, is the set of points $\mathbf{x}$ such that $|\mathbf{F}^k(\mathbf{x}) - \mathbf{F}^k(\mathbf{p})| \to \mathbf{0}$, as $k \to \infty$.

Dynamical System: A dynamical system is a set of states, with a rule that determines the present state in terms of past states. This system can be formulated as:

$$x_n = F(x_{n-1}), \tag{24}$$

where n stands for time, and x_n designate the state of system at time n.

Fixed Point: Let $\mathbf{F}$ be a map on $\Re^m$, $m \geq 1$. Then a point $\mathbf{p}$ in $\Re^m$ is a fixed point of the map $\mathbf{F}$ if $\mathbf{F}(\mathbf{p}) = \mathbf{p}$.

Hyperbolic Fixed Point: A fixed point $\mathbf{p}$ is called **hyperbolic** if none of the eigenvalues of $\mathbf{DF}(\mathbf{p})$ (see Jacobian matrix) has magnitude 1.

Inverse Maps: Map $\mathbf{F}$ has an inverse map $\mathbf{F}^{-1}$ if it is a one-to-one map.

Jacobian Matrix: Let $\mathbf{F} = (F_1,\ F_2,\ \cdots,\ F_m)$ be a map on $\Re^m$, and let $\mathbf{p} \in \Re^m$.

The Jacobian matrix of $\mathbf{F}$ at $\mathbf{p}$, denoted by $\mathbf{DF}(\mathbf{p})$, is the matrix

$$\mathbf{DF}(\mathbf{p}) = \begin{bmatrix} \frac{\partial F_1(\mathbf{p})}{\partial x_1} & \frac{\partial F_1(\mathbf{p})}{\partial x_2} & \cdots & \frac{\partial F_1(\mathbf{p})}{\partial x_m} \\ \\ \frac{\partial F_2(\mathbf{p})}{\partial x_1} & \frac{\partial F_2(\mathbf{p})}{\partial x_2} & \cdots & \frac{\partial F_2(\mathbf{p})}{\partial x_m} \\ \\ \cdot & \cdot & & \cdot \\ \cdot & \cdot & & \cdot \\ \cdot & \cdot & & \cdot \\ \frac{\partial F_m(\mathbf{p})}{\partial x_1} & \frac{\partial F_m(\mathbf{p})}{\partial x_2} & \cdots & \frac{\partial F_m(\mathbf{p})}{\partial x_m} \end{bmatrix} \tag{25}$$

of partial derivatives evaluated at $\mathbf{p}$.

Manifold: An m-dimensional manifold is a set that locally resembles Euclidean space $\Re^m$ in a topological sense. Each point of a manifold must have a neighbourhood around itself that looks like $\Re^m$. A 1-dimensional manifold is locally a curve (like letters **D** and **o** not letters **A** and **X**). The surface of oranges and doughnuts are examples of 2-dimensional manifolds. 1-dimensional manifolds does not include open curves like letters **L** and **U** because of their endpoints. This type of set is called a **manifold with boundary**, although technically it is not a manifold.

Map: A function whose domain (input) and range (output) space are the same will be called a map. Assume x as a set of points, and $F(x)$ as a map. As a result, x and $F(x)$ have the same set.

One-to-One Map: A map $\mathbf{F}$ on $\Re^m$ is **one-to-one** if $\mathbf{F}(\mathbf{v_1}) = \mathbf{F}(\mathbf{v_2})$ implies $\mathbf{v_1} = \mathbf{v_2}$.

Orbit: The orbit of x under F is the set of points $\{x,\ F(x),\ F^2(x),\ \cdots\}$. The starting point of x for the orbit is called the initial value of the orbit.

Periodic Orbit: An orbit with initial point p which consists of K points such that $x_K = p$ is called a **periodic orbit of period** K or, more briefly, **period-K orbit**.

Periodic Points: Let F be a map on $\Re$. Point p is called a periodic point of period K if $F^K(p) = p$, and if K is the smallest such positive integer. The term **period-K point** is the abbreviated form.

Repelling Fixed Point: Let F be a map on $\Re$, and let p be a real number such that $F(p) = p$. If all points sufficiently close to p are repelled from p, then p is called a repelling fixed point or source. In other words, if there is an $\epsilon > 0$ neighbourhood of p, $\mathcal{U}_\epsilon(p)$, such that each x in $\mathcal{U}_\epsilon(p)$ except for p itself eventually maps outside of $\mathcal{U}_\epsilon(p)$, then p is a source. For a smooth map on $\Re$ with the fixed point of p, if $|F'(p)| > 1$, then p is source.

In multidimensional case, let $\mathbf{F}$ be a map on $\Re^m$, and let $\mathbf{p}$ be in $\Re^m$ such that $\mathbf{F}(\mathbf{p}) = \mathbf{p}$. If there is an ϵ-neighbourhood of $\mathbf{p}$, $\mathcal{U}_\epsilon(\mathbf{p})$, such that each $\mathbf{v}$ in $\mathcal{U}_\epsilon(\mathbf{p})$

except for $\mathbf{p}$ itself eventually maps outside of $\mathcal{U}_\epsilon(\mathbf{p})$, then $\mathbf{p}$ is a repeller or source. If the magnitude of each eigenvalue of $\mathbf{F}'(\mathbf{p})$ (see Jacobian matrix) is greater than 1, then $\mathbf{p}$ is a source.

Saddle Fixed Point: If $\mathbf{p}$ is hyperbolic and if at least one eigenvalue of $\mathbf{DF}(\mathbf{p})$ (see Jacobian matrix) has magnitude greater than 1, and at least one eigenvalue has magnitude less than 1, then $\mathbf{p}$ is called a **saddle**. Saddles points are unstable, i.e., almost any perturbation of the orbit away from the fixed point will be magnified under iterations.

Sink: See Attracting Fixed Point.

Source: See Repelling Fixed Point